Generation of homogeneous rhodium particles by photoreduction of Rh(III) on TiO2 colloids grafted on SiO2

ARTICLE *in* LANGMUIR · JANUARY 1993

Impact Factor: 4.46 · DOI: 10.1021/la00025a028

5 AUTHORS, INCLUDING:

Agustin R. Gonzalez-Elipe
Spanish National Research Council
434 PUBLICATIONS **7,300** CITATIONS
SEE PROFILE

C. Real
Spanish National Research Council
104 PUBLICATIONS **1,422** CITATIONS
SEE PROFILE

Alfonso Caballero
Universidad de Sevilla
119 PUBLICATIONS **2,373** CITATIONS
SEE PROFILE

G. Munuera
Universidad de Sevilla
119 PUBLICATIONS **3,549** CITATIONS
SEE PROFILE

Generation of Homogeneous Rhodium Particles by Photoreduction of Rh(III) on TiO_2 Colloids Grafted on SiO_2

A. Fernández,* A. R. González-Elipe, C. Real, A. Caballero, and G. Munuera

Instituto de Ciencia de Materiales and Departamento Química Inorgánica, Universidad de Sevilla, P.O. Box 1115, 41080 Sevilla, Spain

Received September 12, 1991. In Final Form: August 27, 1992

Three TiO_2/SiO_2 samples (3, 6, and 12 wt % TiO_2) have been prepared by reaction of OH groups and water of the SiO_2 surface with $Ti(OCH(CH_3)_2)_4$. Characterization of the materials by X-ray diffraction (XRD), diffuse reflectance spectroscopy (DRS), X-ray photoelectron spectroscopy (XPS), and EXAFS/XANES indicates the existence of TiO_2 grafted on the surface of the SiO_2 in the form of very small amorphous particles ($d \leq 30$ Å), showing quantum size effects. The photochemical deposition of rhodium on these TiO_2/SiO_2 materials has been studied. Characterization by XRD, XPS, and transmission electron microscopy (TEM) of the resulting $Rh–TiO_2/SiO_2$ composite materials shows the formation of small metallic particles with very narrow size distributions which depend on the amounts of titania grafted on the SiO_2 and on the initial concentration of rhodium in solution. A mechanism is proposed to explain the photochemically controlled growth of the colloidal Rh particles on the TiO_2/SiO_2 supports.

Introduction

Small particles of different semiconductor materials can now be prepared in a variety of media including solutions,[1-3] glasses,[4] zeolites,[5] and polymers.[6] The study of the properties and behavior of such colloidal semiconductor particles in porous and nonporous matrices has lead to many applications in different fields such as heterogeneous catalysis,[7] photocatalysis,[8] nonlinear optic devices,[6] etc.

A common practice in catalysis consists of the dispersion of the active phase on a carrier of high surface area like SiO_2 or Al_2O_3.[9] Thus, small TiO_2 particles supported on SiO_2 have been synthesized by different researchers[10-12] by reacting alkoxides, e.g., $Ti(OR)_4$, with surface hydroxyl groups of the SiO_2, a process that Muñoz et al.[12] have recently examined showing the role of adsorbed water on the grafting process.

On the other hand, although the photocatalytic activity of TiO_2 in bulk or colloidal form has been widely studied for a great variety of reactions[13] that include the photochemical reduction of noble metals,[14-19] less work has been done for colloidal TiO_2 supported on a nonphotoactive substrate. In this case Herrmann et al.[20] have shown, using analytical transmission electron microscopy (TEM), that Pt is selectively photoreduced on the supported titania.

In the present paper we describe the synthesis and spectroscopic characterization of quantum-sized TiO_2 colloidal particles supported on silica together with the photochemical deposition of metallic rhodium on these materials. From the characterization of the resulting $Rh–TiO_2/SiO_2$ samples a mechanism for the homogeneous growth of the metallic particles produced by the photocatalytic process has been worked out.

Experimental Section

Synthesis of TiO_2/SiO_2 Supports. Three TiO_2/SiO_2 samples containing 3, 6, and 12 wt % TiO_2 (hereafter $TiO_2(3)/SiO_2$, $TiO_2(6)/SiO_2$, and $TiO_2(12)/SiO_2$, respectively) were prepared by incipient wetness impregnation of SiO_2 (Aerosil, $S_{BET} = 200$ $m^2 \cdot g^{-1}$) with a *n*-hexane (Merck pa) solution of $Ti(OCH(CH_3)_2)_4$ (Tilcom). After drying in air for 14 h at 295 K and for 24 h at 373 K, the materials were calcined in air at 873 K for 10 h. For comparative purposes another three samples were prepared as physical mixtures containing SiO_2 and 3, 6, and 12 wt % TiO_2 (Degussa P-25, 50 $m^2 \cdot g^{-1}$). The samples will be designated hereafter as $TiO_2(3) + SiO_2$, $TiO_2(6) + SiO_2$, and $TiO_2(12) + SiO_2$, respectively.

Rhodium Photoreduction. Two series of samples were prepared by photodeposition of 1 and 2 wt % rhodium on each of the three TiO_2/SiO_2 supports. The resulting materials, with Rh:Ti atomic ratios ranging from 0.06 to 0.50, will be named here

(1) Brus, L. E. *J. Phys. Chem.* **1986**, *90*, 2555 and references therein.
(2) Ramsden, J. J.; Webber, S. E.; Grätzel, M. *J. Phys. Chem.* **1985**, *89*, 2740.
(3) Weller, H.; Schmidt, H. M.; Koch, V.; Fojtik, A.; Baral, S.; Henglein, A.; Kunath, W.; Weiss, K.; Dieman, E. *Chem. Phys. Lett.* **1986**, *124*, 557 and references therein.
(4) Ekimov, A. I.; Efros, H. L.; Onushchenko, A. *Solid State Commun.* **1985**, *56*, 921.
(5) Wang, Y.; Herron, N. *J. Phys. Chem.* **1987**, *91*, 257.
(6) Wang, Y.; Mahler, W. *Opt. Commun.* **1987**, *61*, 233.
(7) Fernández, A.; Leyrer, J.; González-Elipe, A. R.; Munuera, G.; Knözinger, H. *J. Catal.* **1988**, *112*, 489.
(8) Spanhel, L.; Weller, H.; Henglein, A. *J. Am. Chem. Soc.* **1987**, *109*, 6632.
(9) Che, M.; Tench, A. *J. Adv. Catal.* **1984**, *32*, 1.
(10) a) Matsuo, K.; Nakano, K. *Appl. Surf. Sci.* **1988**, *33/34*, 269. b) McDaniel, M. P.; Welch, M. B.; Dreiling, M. J. *J. Catal.* **1983**, *82*, 118.
(11) a) Reichmann, M. G.; Bell, A. T. *Appl. Catal.* **1987**, *32*, 315. b) Reichmann, M. G.; Bell, A. T. *Langmuir* **1987**, *3*, 111.
(12) Muñoz, A.; Munuera, G. *Stud. Surf. Sci. Catal.* **1991**, *63*, 627.
(13) a) Kiwi, J.; Borgarello, E.; Pelizzetti, E.; Visca, M.; Grätzel. M. In *Photogeneration of Hydrogen*; Harriman, A., West, M. A., Eds.; Academic Press: New York, 1982; p 119. b) Sakata, T.; Kawai, T. In *Energy Resources through Photochemistry and Catalysis*; Grätzel, M., Ed.; Academic Press: New York, 1983; p 331. c) Borgarello, E.; Kiwi, J.; Grätzel, M.; Pelizzetti, E.; Visca, M. *J. Am. Chem. Soc.* **1982**, *104*, 2996.
(14) a) Borgarello, E.; Serpone, N.; Emo, G.; Harris, R.; Pelizzetti, E.; Minero, C. *Inorg. Chem.* **1986**, *25*, 4499. b) Borgarrello, E.; Harris, R.; Serpone, N. *Nouv. J. Chim.* **1985**, *9*, 743. c) Serpone, N.; Borgarrello, E.; Pelizzetti, E. In *Photocatalysis and Environment*; Schiavello, M., Ed.; NATO ASI Series C; Kluwer: Dordrecht, The Netherlands; Vol. 237, p 527.
(15) Bickley, R. L. In *Catalysis*; Kembal, C., Ed.; The Chemical Society: London, 1982; p 308.
(16) Stadler, K. H.; Boehm, H. P. *Proceedings of the 8th International Congress on Catalysis*; Verlag Chemie: Weinheim, FRG, 1984; Vol. IV, p 803.
(17) a) Herrmann, J.-M.; Disdier, J.; Pichat, P. *J. Phys. Chem.* **1986**, *90*, 6028. b) Herrmann, J.-M.; Disdier, J.; Pichat, P.; Leclercq, C. In *Preparation of Catalysts IV*; Delmond, B., et al., Eds.; Elsevier: Amsterdam, 1987; p 285.
(18) a) Krauetler, B.; Bard, A. J. *J. Am. Chem. Soc.* **1978**, *100*, 4317. b) Dunn, W. W.; Bard, A. J. *Nouv. J. Chim.* **1981**, *5*, 651. c) Sungbom, C., Kawai, M., Tanaka, K. *Bull. Chem. Soc. Jpn.* **1984**, *57*, 871.
(19) a) Fernández, A.; Munuera, G.; González-Elipe, A. R.; Espinós, J. P.; Herrmann, J.-M.; Pichat. P.; Leclercq, C. *Appl. Catal.* **1990**, *57*, 19. b) Herrmann, J.-M.; Disdier, J.; Pichat, P., Fernández, A.; González-Elipe, A. R.; Munuera, G.; Leclercq, C. *J. Catal.* **1991**, *132*, 490.
(20) Herrmann, J.-M.; Mansot, J.-L. *J. Catal.* **1990**, *121*, 340.

0743-7463/93/2409-0121$04.00/0

Table I. S_{BET} ($m^2 \cdot g^{-1}$) Data for TiO_2/SiO_2 and $TiO_2 + SiO_2$

	3 wt % TiO_2	6 wt % TiO_2	12 wt % TiO_2
TiO_2/SiO_2	206	203	205
$TiO_2 + SiO_2$	198	195	188

after as Rh(1)–TiO_2(3)/SiO_2, Rh(1)–TiO_2(6)/SiO_2 Rh(1)–TiO_2(12)/SiO_2, Rh(2)–TiO_2(3)/SiO_2, Rh(2)–TiO_2(6)/SiO_2, and Rh(2)–TiO_2(12)/SiO_2, respectively. In each experiment 7 g of the corresponding TiO_2/SiO_2 support was dispersed in 220 mL of a $^iPrOH/H_2O$ (10:1 v/v) $Rh(NO_3)_3$ solution containing the appropriate amount (1 or 2 wt % Rh in the final sample) of the metal precursor salt. The suspensions were then irradiated in the absence of oxygen for 3 h in a quartz immersion cell using a mercury arc (400 W). After centrifugation the samples were dried under nitrogen at room temperature and stored in a desiccator.

Methods. X-ray diffractograms were recorded with a Philips PW 1060XR diffractometer, while UV–vis reflectance spectra were measured with a Perkin–Elmer 554 UV–vis spectrometer, equipped with an integration sphere and using SiO_2 as a reference.

X-ray photoelectron spectra were recorded with a Leybold-Heraeus LHS-10 spectrometer working in the $\Delta E = cte$ mode with a pass energy of 50 eV using the Mg $K\alpha$ radiation as an excitation source. The binding energy (BE) reference was taken at the C(1s) line due to carbon impurities at 284.6 eV. A HP 1000E computer on line to the spectrometer was used for data handling (background subtraction and area calculations). Atomic percentages were estimated using sensitivity factors supplied with the spectrometer which are very similar to those reported in the literature.[21]

TEM examinations were performed with a Hitachi H800 microscope. The samples were first ultrasonically dispersed in ethanol, and a drop of this dispersion was deposited on a thin carbon film supported by a copper grid. The electron micrographs were obtained at 200 kV.

The X-ray absorption spectra at the Ti K-edge were collected at the Frascaty Synchrotron Radiation Facility, utilizing the radiation emitted by the storage ring ADONE working at 1.3 GeV with a typical current of 50 mA. The radiation was monochromatized by a Si(111) channel-cut crystal, at an average resolution of 1 eV for the extended X-ray absorption fine structure (EXAFS) spectra and of 0.5 eV for the X-ray absorption near edge (XANES) spectra. The measurements were taken in vacuum at room temperature. The samples in the form of pellets were diluted with boric acid, giving an optical density of the whole set of samples in the range $\mu x = 2.5$.

Results and Discussion

1. Spectroscopic Characterization of TiO_2/SiO_2 Supports. TiO_2 loadings of ca. 3, 6, and 12 wt % were selected by reference to the content corresponding to one monolayer of titania on this type of silica (ca. 12.8 wt % TiO_2[22]). This value is also close to the amount corresponding to the grafting of one Ti atom by one hydroxyl group of the silica surface (13.8 wt % TiO_2, 6 OH/nm^2).[23]

Surface areas (S_{BET}), summarized in Table I, were very similar for the SiO_2 support (Aerosil 200 $m^2 \cdot g^{-1}$) and for the three TiO_2/SiO_2 samples while a small decrease was observed for the physical mixtures as could be expected for the lower surface area of the TiO_2 used as reference (TiO_2, P-25, $S_{BET} = 50\ m^2 \cdot g^{-1}$). These results are indicative of a good dispersion of the TiO_2 grafted on the surface of SiO_2. The X-ray diffraction (XRD) analysis of the samples, shown in Figure 1, confirmed this point since no detectable reflections of crystalline TiO_2 phases were observed for the TiO_2/SiO_2 samples, while the $TiO_2 + SiO_2$ physical mixtures clearly showed the principal diffraction peaks of anatase and rutile typical of the Degussa P-25 product.

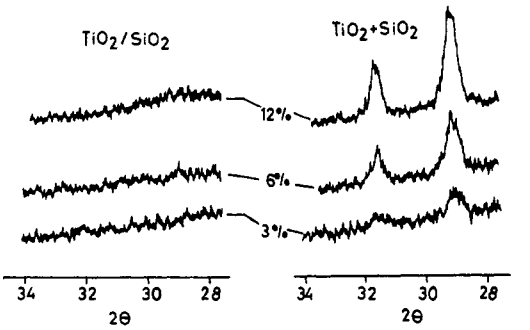

Figure 1. X-ray diffractograms of the TiO_2/SiO_2 and $TiO_2 + SiO_2$ samples with different TiO_2 contents (wt %).

Table II. Ti/Si Atomic Ratios from XPS for TiO_2/SiO_2 and $TiO_2 + SiO_2$

	3 wt % TiO_2	6 wt % TiO_2	12 wt % TiO_2
TiO_2/SiO_2	0.033	0.042	0.063
$TiO_2 + SiO_2$	0.013	0.016	0.038

Further information on the degree of dispersion of the TiO_2 phase was obtained by X-ray photoelectron spectroscopy (XPS). The relative intensities of the Ti(2p) peak of the different TiO_2/SiO_2 samples and the $TiO_2 + SiO_2$ mixtures are summarized in Table II. The values in this table, significantly greater in the former case, clearly confirm the conclusion drawn above from S_{BET} and XRD data, in the sense that the TiO_2 phase is highly dispersed in the TiO_2/SiO_2 samples. In addition, the Ti(2p) spectrum in all these samples was broader than in the $TiO_2 + SiO_2$ mixtures (full width at half-maximum $\simeq$3.0 eV for TiO_2/SiO_2 vs $\simeq$1.6 eV for $TiO_2 + SiO_2$). This effect can be attributed to a greater heterogeneity of the Ti centers as could be expected from an amorphous phase of colloidal titania, though broadening due to charge effects cannot be completely excluded. On the other hand, values of the modified Auger parameter[24] calculated from the Ti(2p) BE and the $TiL_3M_{23}V$ kinetic energy were 872.8 and 870.6 eV for the TiO_2 and TiO_2/SiO_2 samples, respectively. This difference can be accounted for by a difference in the relaxation energy of the photohole of –1.1 eV in TiO_2/SiO_2 with respect to TiO_2 and can be attributed to the nature of the TiO_2–SiO_2 interface (i.e., Ti–O–Si bonding) as we have discussed elsewhere.[25]

More precise details about the structure of the TiO_2 phase have been obtained from X-ray absorption experiments. The XANES region of the Ti K-edge for the TiO_2(12)/SiO_2 and TiO_2(6)/SiO_2 samples has been plotted in Figure 2 together with the corresponding spectra of anatase, rutile, and $Ti(O^iPr)_4$ measured as references. The similar shape of the spectra of the TiO_2 supported samples and that of $Ti(O^iPr)_4$ indicates a similar local structure in both cases. In particle the round shape of features B and C is characteristic of amorphous TiO_2 compounds[26] while the appearance of a triplet and the small intensity of feature A indicate that the Ti atom is 6-coordinated.[27,28]

Fourier transforms of the EXAFS signal for the Ti K-edge are shown in Figure 3 for the TiO_2(12)/SiO_2 and

(21) Wagner, D. C.; Davies, L. E.; Zeller, M. V.; Taylor, J. A.; Raymond, R. M.; Gale, L. H. *Surf. Interface Anal.* **1981**, *3*, 211.
(22) All TiO_2 weight percentages given here are referred to 100 g of the TiO_2/SiO_2 sample.
(23) Barky, D. In *Characterization of powder surfaces*; Parfitt, G. D., Sing, K. S. W., Eds.; Academic Press: New York, 1976; p 407.
(24) Wagner, D. C. *Faraday Discuss. Chem. Soc.* **1975**, *60*, 291.
(25) Fernández, A.; Caballero, A.; González-Elipe, A. R. *Surf. Interface Anal.* **1992**, *18*, 392.
(26) a) Léaustic, A.; Babonneau, F.; Livage, I. *Chem. Mater.* **1989**, *1*, 240. b) *Ibid.*, **1989**, *1*, 248.
(27) Sandstrom, D. R.; Lytle, F. W.; Wei, P. S. P.; Greegor, R. G.; Wong, J.; Schultz, P. *J. Non-Cryst. Solids* **1980**, *41*, 201.
(28) Babonneau, F.; Doeuff, S.; Léaustic, A.; Sánchez, C.; Cartier, C.; Verdaguer, M. *Inorg. Chem.* **1988**, *27*, 3166.

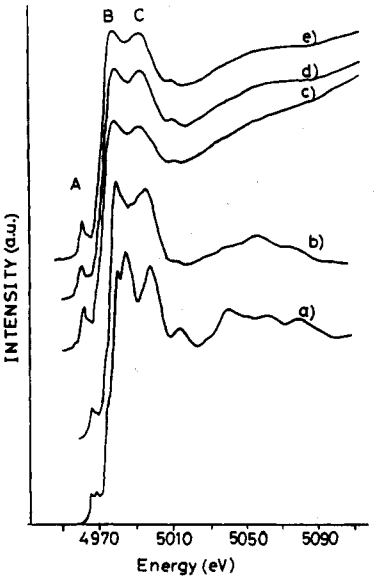

Figure 2. XANES region of the Ti K-edge for (a) rutile, (b) anatase, (c) $Ti(O^iPr)_4$, (d) $TiO_2(6)/SiO_2$, and (e) $TiO_2(12)/SiO_2$.

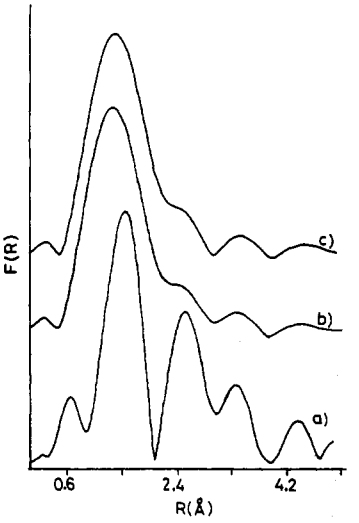

Figure 3. Fourier transforms of the EXAFS spectra of (a) anatase, (b) $TiO_2(6)/SiO_2$, and (c) $TiO_2(12)/SiO_2$ samples.

$TiO_2(6)/SiO_2$ samples and for the TiO_2 anatase as reference compound. The intense peak at around 1.7 Å in all cases is due to the first neighbor oxygen atoms around the Ti. The absence of intense peaks at higher distances ($d > 2.0$ Å) indicates a lack of intermediate and long-range order around the Ti, which is in agreement with the absence of XRD peaks for these samples. Fitting of the EXAFS curves shows that the first peak in the Fourier transform can be attributed to six Ti–O bonds at 1.93 Å, the same distance as the short bond of the distorted octahedra in anatase.[29] The second peak in the Fourier transform corresponds to Ti–Ti distances of 3.08 Å, very similar to those in TiO_2 anatase (3.04 Å) and corresponds to TiO_6 octahedra sharing edges.[29] However, the low coordination number for this second shell ($N = 1$ Ti vs $N = 4$ Ti for anatase) indicates that the TiO_2 aggregates are in the form of small clusters of TiO_6 octahedra highly disordered with a high surface:bulk ratio.

Semiconductor particles of small size present a shift of the absorption edge to lower wavelengths. This shift can be taken as an indication of the particle size and is commonly interpreted as a quantum size effect.[30-33] Figure 4 shows the UV–vis spectra of the TiO_2/SiO_2 samples in comparison with those of the physical $TiO_2 + SiO_2$ mixtures. From this figure it is clear that the absorption edge of the former samples is shifted toward shorter wavelengths, thus supporting the small size of the TiO_2 particles in these samples. A simple calculation (after the paper of Rossetti et al.[30a]) taking into account the increase in e^- and h^+ localization kinetic energies and the attractive electrostatic interaction between e^- and h^+ for an exciton in small cyrstallites give us an upper limit for the titania particle diameter of about 30 Å for the sample with 12% TiO_2, in good agreement with previously reported results.[34]

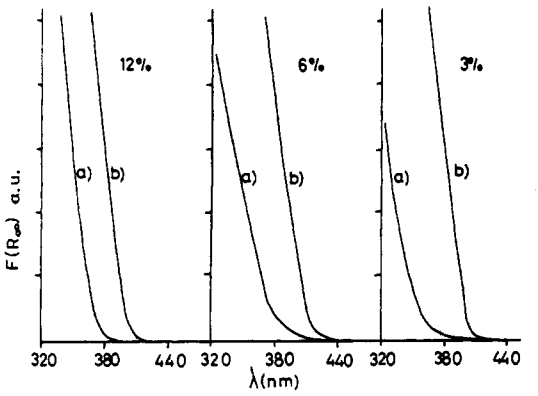

Figure 4. Diffuse reflectance spectra of (a) TiO_2/SiO_2 and (b) $TiO_2 + SiO_2$ samples.

2. Rhodium Photoreduction on TiO_2/SiO_2. Photodeposition of rhodium from an aqueous/alcoholic solution has been examined in detail as a possible way for a taylored synthesis of metal/semiconductor/insulator materials of colloidal dimensions with potential interest as catalysts and chemical sensors.[35]

Irradiation in the absence of O_2 of a white suspension of the $TiO_2(12)/SiO_2$ sample in a $^iPrOH/H_2O$ solution turned the suspension into a deep blue color, not observed when the experiment is carried out using bulk TiO_2 P-25. Under these conditions we can expect that photogenerated holes oxidize the ^iPrOH to acetone[36] while the photoelectrons will reduce the Ti^{4+} ions to Ti^{3+}. The presence of this ion has been associated with the deep blue color developed by these kinds of samples during irradiation or by heating in hydrogen at $T > 723$ K. By comparison with bulk TiO_2 the enhanced photoreducibility of the Ti^{4+} ions of the supported colloids can be ascribed to the increase in the redox potential experienced by the photogenerated carriers in the quantized semiconductor particles so that redox reactions should now be more efficient,[37-39] although electron–hole recombinations will also be enhanced.

(29) Kozlowski, R.; Pettifer, R. F.; Thomas, J. M. *J. Phys. Chem.* **1983**, *87*, 5172.

(30) a) Rosseti, R.; Nakahara, S.; Brus, L. E. *J. Chem. Phys.* **1983**, *79*, 1086. b) Brus, L. E. *J. Chem. Phys.* **1984**, *80*, 4403.

(31) a) Haase, M.; Weller, H.; Henglein, A. *J. Phys. Chem.* **1988**, *92*, 482; b) Bahnemann, D. W.; Kormann, C.; Hoffmann, M. R. *J. Phys. Chem.* **1987**, *91*, 3789.

(32) Kamat, P. V.; Dimitrijevic, N. M. *Sol. Energy* **1990**, *44*, 83.

(33) a) Williams, F.; Nozik, A. J. *Nature (London)* **1984**, *311*, 21. b) Nedeljkovic, J. M.; Nenadovic, M. T.; Micic, O. I.; Nozik, A. J. *J. Phys. Chem.* **1986**, *90*, 12.

(34) Kormann, C.; Bahneman, D. W.; Hoffmann, M. R. *J. Phys. Chem.* **1988**, *92*, 5196.

(35) Morrison, S. R. *Sens. Actuators* **1982**, *2*, 329.

(36) Ait-Ichou, I.; Formenti, M.; Pommier, B.; Teichner, S. I. *J. Catal.* **1985**, *91*, 293.

(37) Nenadovic, M. T.; Nedeljkovic, J. M.; Micic, O. I. *J. Chem. Soc., Faraday Trans. 1* **1987**, *83*, 1127.

(38) Spanhel, L.; Henglein, A.; Weller, H., *Ber. Bunsen-Ges. Phys. Chem.* **1987**, *91*, 1359.

(39) Nozik, A. J.; Williams, F.; Nenadovic, M. T.; Raj, T.; Micic, O. I. *J. Phys. Chem.* **1985**, *89*, 397.

Table III. Average Diameter of Rh Particles for $Rh-TiO_2/SiO_2$

sample	D (Å) TEM	D (Å) XRD	sample	D (Å) TEM	D (Å) XRD
$Rh(1)-TiO_2(12)/SiO_2$	24		$Rh(2)-TiO_2(12)/SiO_2$	45	48
$Rh(1)-TiO_2(6)/SiO_2$	26		$Rh(2)-TiO_2(6)/SiO_2$	52	58
$Rh(1)-TiO_2(3)/SiO_2$	30		$Rh(2)-TiO_2(3)/SiO_2$	62	63

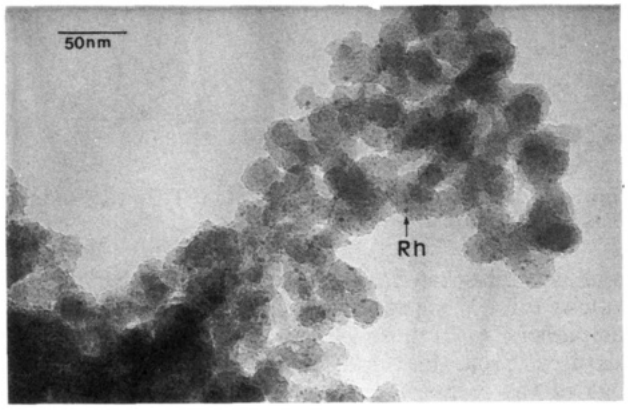

Figure 5. Transmission electron micrograph of the $Rh(1)-TiO_2(12)/SiO_2$ sample.

Irradiation of the TiO_2/SiO_2 materials suspended in a solution of $Rh(NO_3)_3$ in $^iPrOH/H_2O$ produced acetone, as monitored by GC analysis, and metallic rhodium as indicated by the fact that after the reaction completion (i.e., 3 h), no Rh^{3+} could be detected in the solution by UV–vis spectroscopy. The following reaction can be proposed from these observations:

$$3(CH_3)_2CHOH + 2RH^{3+} \rightarrow 3(CH_3)_2CO + 2Rh^0 + 6H^+ \quad (1)$$

The complete photoreduction of the rhodium during the experiments leads to the formation of $Rh-TiO_2/SiO_2$ composite materials, which were further examined by XPS, XRD, and TEM to characterize the colloidal metallic phase.

XPS analysis of the freshly prepared samples shows the presence of metallic rhodium ($Rh(3d_{5/2})$ at a binding energy of 306.7 eV), though storage in air for a few days leads to a partial oxidation of the metal up to Rh^{3+} as could be expected for very small particles.[40]

X-ray diffractograms of the samples containing 2 wt % Rh show diffraction lines characteristic of the metal. From the X-ray diffraction line broadening of the Rh(111) peak, the average particle sizes summarized in Table III were obtained for the materials containing increasing amounts of TiO_2. However, for the samples containing only 1 wt % Rh, X-ray diffraction lines due to the metal could not be detected, thus indicating the formation of much smaller particles.

Figures 5 and 6 show, as an example, the transmission electron micrographs for the $Rh(1)-TiO_2(12)/SiO_2$ and $Rh(2)-TiO_2(3)/SiO_2$ samples, the two extreme situations of high and low metal dispersion. From an exhaustive TEM analysis of the different samples the rhodium particle size distributions depicted in Figure 7, together with the mean particle diameters summarized in Table III, were obtained. A very good agreement with XRD values exists.

Two important features must be stressed from these results: (i) Metal particle sizes present a very narrow distribution for the two sets of samples (e.g., 1 and 2 wt % Rh, Figure 7). (ii) The metal particle size decreases for TiO_2/SiO_2 samples with a higher TiO_2 content (Table III).

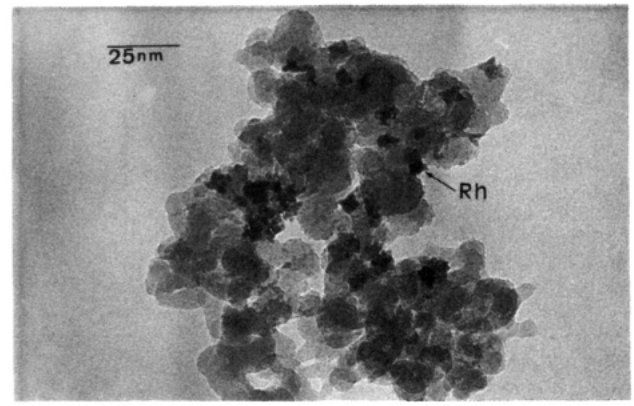

Figure 6. Transmission electron micrograph of the $Rh(2)-TiO_2(3)/SiO_2$ sample.

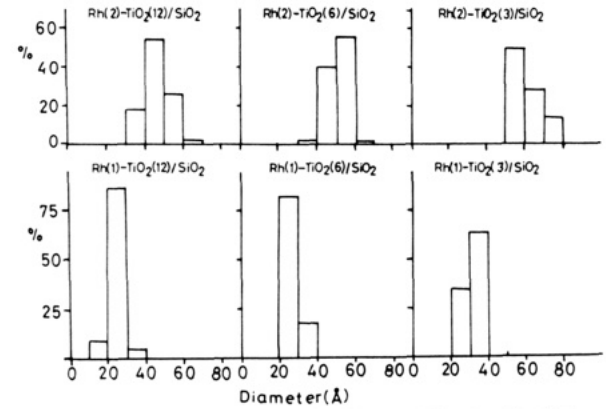

Figure 7. Size distribution of the Rh particles for the different $Rh-TiO_2/SiO_2$ samples (the *Y* axis represents percentage of particles).

In addition, it is noteworthy that for the two sets of samples (1 and 2 wt % Rh) very different distributions of particles are observed in the TEM micrographs. In the low loaded materials a great number of homogeneously dispersed particles is observed while for the 2 wt % Rh loaded set, bigger particles are observed but in a smaller number.

3. Mechanism for Rh(III) Photoreduction. The overall equation (eq 1) for photoreduction of rhodium can be decomposed in the following steps: (i) oxidation of ^iPrOH by the photoproduced holes[36]

$$^3/_2(CH_3)_2CHOH + 3h^+(TiO_2) \rightarrow {}^3/_2(CH_3)_2CO + 3H^+ \quad (2)$$

(ii) reduction of metal cations by the semiconductor free electrons to form zerovalent metal atoms[16]

$$Rh^{3+} + 3e^-(TiO_2) \rightarrow Rh^0(ads) \quad (3)$$

(iii) spontaneous agglomeration of zerovalent rhodium atoms into small clusters, a process that, according to Herrmann et al.,[17] may occur either involving other metal atoms or via cathodic-like reduction at primary metallic nuclei

$$Rh^0 + Rh^{3+} \rightarrow (Rh_2)^{3+} \xrightarrow{+3e^-} Rh_2{}^0 \xrightarrow{+Rh^{3+}} (Rh_3)^{3+} \rightarrow \xrightarrow{+3e^-} Rh_3{}^0 \xrightarrow{+Rh^{3+}} \ldots \rightarrow Rh_m \quad (4)$$

In our case, the amount of TiO_2 on the SiO_2 seems to determine the number of initial "sites" generated by irradiation where the Rh^{3+} photoreduction occurs to form "metallic nuclei". Thus, for the same amount of rhodium,

(40) Muñoz, A.; Munuera, G.; Malet, P.; González-Elipe, A. R.; Espinós, J. P. *Surf. Interface Anal.* **1988**, *12*, 247.

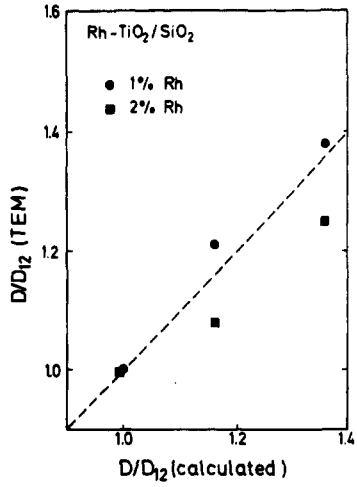

Figure 8. TEM diameter of the Rh particles (normalized for $Rh-TiO_2(12)/SiO_2$ values) vs values calculated assuming cathodic-like growth of small nuclei (see text).

the samples with higher TiO_2 loadings will have more metallic nuclei that then growth to form bigger particles until the total amount of Rh^{3+} in solution has been consumed. This explains that the higher the TiO_2 loading the lower the particle sizes in the two sets of samples (1 and 2 wt % Rh).

If we assume that, during an initial fast photonucleation, small Rh clusters (probably formed only of a few atoms) are generated and that their number is, for each sample, proportional to the surface exposed by the grafted TiO_2 colloids (in principle proportional to the $^2/_3$ root of the TiO_2 weight), the relative sizes of the metallic particles can be calculated, assuming cathodic-like reduction on the nuclei of the remaining Rh^{3+}, and compared with those obtained from TEM/XRD in Table III. Figure 8 shows the values calculated in this way compared with the data deduced from TEM. For the set of samples with 2 wt % Rh the data fit quite well with the values predicted by this simple model, though for the samples with 1 wt % Rh they are slightly lower. For this second set of samples the particle sizes are in the range 24–30 which corresponds to 300–560 Rh atoms for polyhedral-shaped Rh particles.[41] If we assume only cathodic-like photodeposition, the addition of 1 wt % Rh^{3+} for instance to the sample $Rh(1)-TiO_2(12)/SiO_2$ to reach a 2 wt % Rh loading would increase the particle sizes from 24 to 30 Å (from ca. 300 to 600 Rh atoms), far from the 48 Å observed by TEM for the sample $Rh(2)-TiO_2(12)/SiO_2$. So, we must conclude that the number of nuclei in the set of samples containing 2 wt % Rh should be lower than in the corresponding materials with 1 wt % Rh, thus allowing greater particle sizes. From the TiO_2 and Rh loadings in the sample $Rh(1)-TiO_2(12)/SiO_2$ we can calculate a ratio of the number of metallic particles (D_{12} = 24 Å, ca. 300 Rh atoms) to Ti^{4+} ions of ca. 2×10^{-4} which can be compared with the initial $Rh^{3+}:Ti^{4+}$ ratio for this sample of ca. 6×10^{-2}. So, only ca. 1% of the Ti^{4+} act as effective "reduction sites" where Rh nuclei grow to form metallic particles, a number that should be much lower in the samples with 2 wt % Rh.

In addition, it is noteworthy that the ratio of the diameters of the metallic particles on a similar support in both sets of samples ($D(2\%)/D(1\%)$) is ca. 2. This ratio is also greater than that calculated from the Rh loading ($D(2\%)/D(1\%) = 1.27$) assuming the same number of nuclei, which confirms that two different mechanisms have been operating in the generation of the Rh particles in the two sets of samples.

In principle, the above differences in the growth of the Rh particles in the two sets of materials can be explained if the initial fast photonucleation generates a great number of very small metallic clusters which, in the case of the 1 wt % loaded samples, consume most of the Rh^{3+} from the solution (particularly in the case of the higher TiO_2 loaded support). This effect favors the growth of these nuclei mainly by surface diffusion of the clusters which leads to a great number of small particles, in the range 24–30 Å, with very narrow size distributions as observed by TEM in Figure 5. However, for the samples with 2 wt % Rh part of the Rh^{3+} still remains in solution after the initial nucleation, which will favor its cathodic-like photoreduction on a small fraction of the original nuclei, thus leading to much bigger particles (ca. 48–62 Å), which now appear highly dispersed in the support as shown in the TEM micrograph of Figure 6.

Conclusions

Well-dispersed amorphous titania colloids ($d \leq 30$ Å) grafted on SiO_2 have been prepared and characterized by XRD, XANES/EXAFS, and UV–vis absorption spectra as highly amorphous colloids of very small size tightly bonded to the SiO_2 support.

Rhodium photoreduction on these TiO_2/SiO_2 materials leads to samples with a very homogeneous size distribution of metallic particles. The generation and growth of this metallic phase can be explained by assuming that, in a first step, a certain number of reduction sites on the UV-irradiated TiO_2 colloids occur where small metallic nuclei of Rh are formed which is followed by a homogeneous growth of these nuclei either by their diffusion at the surface or by cathodic-like reduction of Rh^{3+} in solution depending on the initial conditions. Composite materials with very well controlled metallic particle sizes can be prepared in this way, changing the amounts of TiO_2 and Rh^{3+}.

Acknowledgment. The authors thank the CICYT (Project Mat88-0223) for financial support, the PWA laboratory staff for technical assistance, and the facilities given by the Electron Microscopy Service of Seville University.

Registry No. TiO_2, 13463-67-7; SiO_2, 7631-86-9; Rh, 7440-16-6; $Ti(OCHMe_2)_4$, 546-68-9; ^iPrOH, 67-63-0.

(41) Benfield, R. E. Personal communication.